Novel thick-target inverse kinematics method for the astrophysical ^{12}C + ^{12}C fusion reaction[*]

Wei-Ke Nan,[1] You-Bao Wang,[1, †] Yao-De Sheng,[2] Jun Su,[2, 3, ‡] Yu-Qiang Zhang,[1] Lu-Yang Song,[2] Yang-Ping Shen,[1] Fu-Qiang Cao,[1] Chen Chen,[1] Chao Dong,[1] Yun-Ju Li,[1] Zhi-Hong Li,[1] Gang Lian,[1] Wei Nan,[1] Qiang Wang,[1] Na Song,[1] Sheng-Quan Yan,[1] Seng Zeng,[1] Qi-Wen Fan,[1] Hao Zhang,[2] Ming-hao Zhu,[1] Bing Guo,[1,4] and Wei-Ping Liu[1,5, §]

[1]*China Institute of Atomic Energy, P. O. Box 275(10), Beijing 102413, China*
[2]*Key Laboratory of Beam Technology and Material Modification of Ministry of Education,*
College of Nuclear Science and Technology, Beijing Normal University, Beijing 100875, China
[3]*Institute of Radiation Technology, Beijing Academy of Science and Technology, Beijing 100875, China*
[4]*School of Physics, Xi'an Jiaotong University, Xi'an 710049, China*
[5]*Department of Physics, Southern University of Science and Technology, Shenzhen 518055, China*

The ^{12}C + ^{12}C fusion is one of the most important reactions in modern nuclear astrophysics. The trend and magnitude of the reaction rate within the Gamow window strongly influence various astrophysical processes. However, direct measurement of this reaction is extremely difficult, which makes it necessary to develop indirect methods. In this study, the ^{23}Na + p reaction system was used to study the compound nucleus ^{24}Mg. We employed a thick-target inverse kinematics method combined with the γ-charged-particle coincidence technique to measure the proton and α exit channels of ^{24}Mg. Technical details of the ^{23}Na + p thick-target inverse kinematics experiment and analysis are presented herein.

Keywords: Nuclear astrophysics, ^{12}C + ^{12}C fusion reaction, Thick-target inverse kinematics method, γ-charged particle coincidence

I. INTRODUCTION

^{12}C + ^{12}C fusion reactions play a crucial role in various stellar burning scenarios [1–3], particularly during the final stages of massive star evolution, Type Ia supernovae events [4, 5], and superbursts [6, 7]. Hence, many direct measurements, primarily employing charged particles [8–10] and gamma ray spectroscopy [11–13], have been conducted to study nuclear astrophysical reaction rates [14]. Because the Coulomb barrier height for the ^{12}C + ^{12}C system, at approximately 7.5 MeV, is significantly higher than the Gamow window energy ($E_{c.m.} = 1.5 \pm 0.3$ MeV), the cross-section decreases rapidly to below one nanobarn in the energy region of interest. This makes it extremely difficult to measure the ^{12}C + ^{12}C fusion reaction directly within the Gamow energy region. A series of direct measurement data [9, 12, 13, 15] suggests the existence of sub-barrier resonances in the ^{12}C + ^{12}C fusion reaction, leading to an increase in the S-factor as the energy decreases below 2.5 MeV in the frame of the center of mass. Therefore, simple low-energy extrapolation based on high-energy data cannot accurately describe the reaction cross-section within the Gamow energy region.

The ^{12}C+^{12}C fusion reaction rate is mainly contributed by ^{12}C(^{12}C, p)^{23}Na, ^{12}C(^{12}C, α)^{20}Ne, and ^{12}C(^{12}C, n)^{23}Mg. The contribution of the neutron emission channel is marginal because of its negative Q value [16]. In 2018, the Trojan horse method (THM) was employed to measure the S factor of the ^{12}C + ^{12}C fusion reaction at $E_{c.m.} < 2.7$ MeV [17]. To date, this is the only measurement that has entered the Gamow window. The astrophysical S* factor derived from the experiment is much larger than the values of the compilation [18] and various phenomenological and microscopic models [19], such as wave-packet dynamics (TDWP) [20], and coupled channel calculations, such as CC-M3Y+Rep [21, 22]. By contrast, Jiang et al. [23] proposed a hindrance model [24, 25] that showed the opposite trend in the energy region of interest. Despite extensive experimental and theoretical efforts, the exact behavior of the ^{12}C + ^{12}C fusion reaction remains unclear on the existence of resonances or not, particularly in the Gamow window.

Thick-target inverse kinematics (TTIK) is a novel experimental method that has been widely used in radioactive ion beam measurements [26, 27] over the last two decades. In the TTIK measurement, the excitation function is obtained in a one-shot experiment with a single-beam energy. Despite the simplicity of its experimental setup, it has been proven by many measurements [28–35] that a satisfactory resolution of the excitation function can be obtained owing to the inverse kinematics enhancement.

Proton resonance scattering induced by radioactive secondary beams has been investigated [36] with the TTIK method at CIAE since 2005. A series of measurements were conducted for ^{12}C+p, ^{13}N+p, ^{17}F+p, and ^{22}Na+p using stable and radioactive ion beams [37–42]. In this study, we extend the conventional TTIK method to complex exit channels for the first time using γ-charged particle coincidence spectroscopy and demonstrate its applicability to simultaneously extracting the excitation functions of different reaction channels.

II. EXPERIMENT SETUP

The experiment was performed in the HI-13 tandem accelerator laboratory [43–47] at the China Institute of Atomic Energy (CIAE) in Beijing. Fig. 1 illustrates the experimental setup for the ^{23}Na + p thick-target experiments. A beam of 110 MeV ^{23}Na^{9+} ions, with a current of approximately 0.2 enA, was directed onto a $(CH_2)_n$ target with a thickness of $5.8\,\mathrm{mg/cm^2}$, resulting in an energy loss of approximately 66 MeV. Finally, the ^{23}Na ions were fully stopped in a $15.7\,\mathrm{mg/cm^2}$-thick carbon target. Because a high-energy Na beam can easily undergo fusion-evaporation reactions with the carbon atoms in the target, a thick carbon target was used to measure the background.
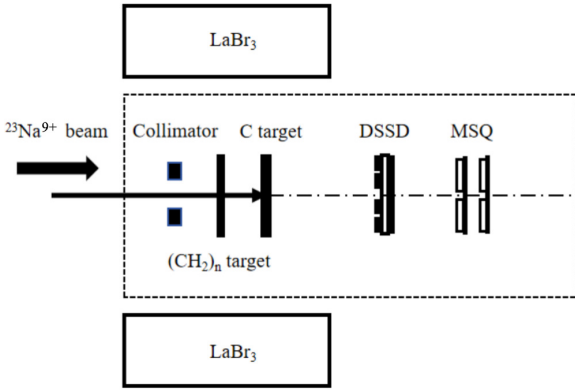

Fig. 1. (Color online) Experimental setup.

A silicon telescope system was placed at 0° along the beamline to measure the protons and α particles emitted from the compound nucleus ^{24}Mg. The silicon telescope system consisted of a 70 μm double-sided silicon strip detector (DSSD), a 1.5 mm multi-guard silicon quadrant (MSQ), and a 1 mm MSQ. The DSSD has 16 strips on each side, dividing the entire Si surface into 256 pixels. The small detection unit of the DSSD provided high-precision angular resolution during the kinematic reconstruction of the charged particles. The charged particles of interest originating from the ^{23}Na + p reaction primarily deposited energy in the first MSQ, and the signals from the second MSQ were used as anti-coincidence signals to reduce the background of high-energy protons and α particles. The wall of the target chamber was made of organic plastic to minimize absorption of the emitted γ rays. Six 3-inch lanthanum bromide detectors were uniformly arranged around the target chamber and placed on sliding rails to allow movement along the vertical beam direction to measure the characteristic γ rays from the residual nuclei ^{23}Na and ^{20}Ne.

III. γ-PARTICLE COINCIDENCE TECHNIQUE

A. LaBr$_3$ detector array calibration

A three-component γ source of ^{60}Co, ^{137}Cs, and ^{241}Am was used to calibrate the LaBr$_3$ array. The Geant4 package [48] was also applied to simulate the efficiency curves of the LaBr$_3$ detectors. The simulation of γ-ray energy spectrum of ^{60}Co was compared with the measured data, as shown in Fig. 2. Using this set of simulation parameters, the efficiency of γ detectors at different energies was obtained. The efficiency curves of the LaBr$_3$ detectors were fitted using Eq. (1) [49], considering several points in the simulation, as shown in Fig. 3. The systematic error in the simulation process was approximately 3 %.
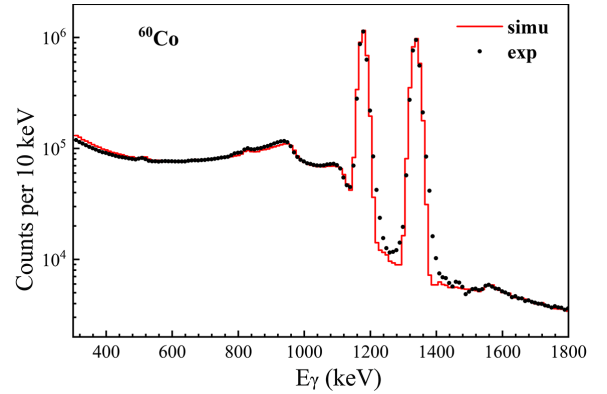

Fig. 2. (Color online) Geant4 simulation for ^{60}Co γ source

$$ln\,\eta(E) = \sum_{i=0}^{n} a_i [lnE]^i, \qquad (1)$$

For the residual nuclei ^{23}Na and ^{20}Ne, the full-energy peak efficiencies at the characteristic energies of 440 and 1634 keV were 28.2 % and 12.6 %, respectively.
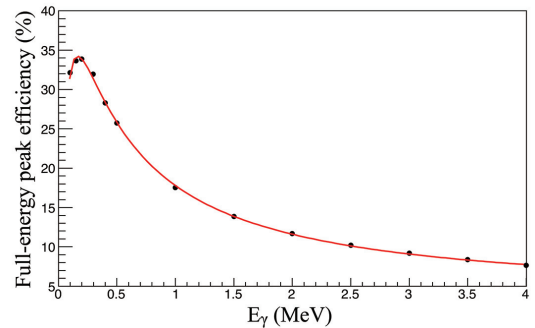

Fig. 3. (Color online) Efficiency curve of the LaBr$_3$ array. The black points are the full-energy peak efficiency of the LaBr$_3$ array for γ rays of different energies obtained from Geant4 simulations. The red line represents the fitting result.

B. γ-charged particle coincidence

The γ background originates mainly from the fusion-evaporation reaction of the high-energy ^{23}Na beam with a carbon target nucleus. For the exit channel p_1 of the compound nucleus, its residual nucleus ^{23}Na emits 440 keV characteristic γ rays, that is, corresponding to the first excited state of ^{23}Na. Because of the large number of γ-high-energy proton accidental coincidence events, it is difficult to quantitatively analyze the p_1 exit channel based on purely γ-charged particle coincidence. The black and red lines shown in Fig. 4 represent the γ energy spectra associated with the proton emissions. After subtracting the C-induced background and correcting for a γ efficiency of 440 keV, the absolute counts of the p_1 channel were obtained.
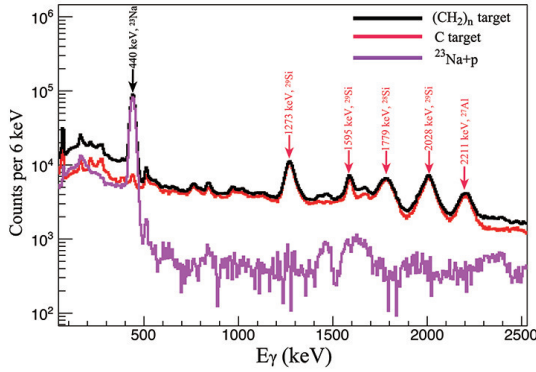

Fig. 4. (Color online) γ ray single energy spectrum measured with the LaBr$_3$ detector array in coincidence with protons. The γ spectrum obtained with (CH$_2$)$_n$-target and carbon-target are presented as black and red lines, respectively. The purple line is the net count spectrum obtained by subtracting the carbon background spectrum after beam normalization.

IV. TWO-BODY KINEMATICS RECONSTRUCTION

The energy spectrum of charged particles obtained by a silicon detector is a mixture of a series of excitation function effects. Because γ-charged-particle coincidence introduces a large number of interfering events originating from the carbon-induced background, it is necessary to subtract these effects from the energy spectrum. In the energy range of the measurement, the exit channels of the compound ^{24}Mg consist of p_0, p_1, α_0, and α_1. Taking the p_0 exit channel as an example, the detailed processing steps for the two-body kinematic reconstruction are outlined below.

Step 1: Extract the energy spectrum of the proton exit channels from the total proton energy spectrum obtained by the silicon detectors after particle identification and energy calibration. The energy spectrum of the p_1 exit channel can be obtained from the charged particle spectrum of the silicon detector via γ_1-proton coincidence. After subtracting the p_1 energy spectrum corrected by γ efficiency from the total

proton energy spectrum, the energy spectrum of p_0 can be obtained. At this stage, both the p_0 and p_1 exit-channel energy spectra contain C-induced backgrounds. Therefore, the proton energy spectrum obtained from the carbon target must be analyzed in a similar manner.
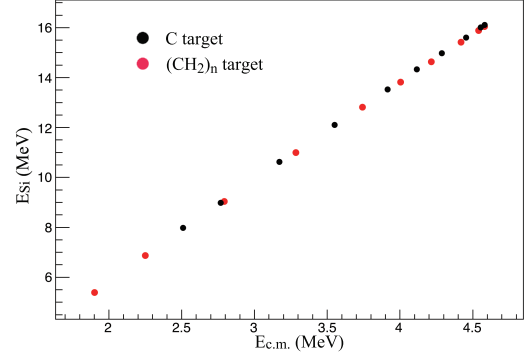

Fig. 5. (Color online) Relationship between $E_{\text{c.m.}}$ and the deposited energy in silicon for the p_1 exit channel.

Step 2: Perform an event-by-event two-body kinematic reconstruction based on where the reaction ^{23}Na$(p, p\gamma_1)^{23}$Na occurs within the thick target and calculate the relationship between $E_{\text{c.m.}}$ and the energy deposited in the silicon detectors. Through energy-loss calculations and reaction kinematics, the energy deposition in the silicon detectors E_{Si} of protons is attributed to $E_{\text{c.m.}}$ of the ^{23}Na$(p, p\gamma_1)^{23}$Na reaction. As shown in Fig. 5, the red and black dots represent the correspondence between E_{Si} and $E_{\text{c.m.}}$ for the ^{23}Na$(p, p\gamma_1)^{23}$Na reaction on the (CH$_2$)$_n$ and carbon target, respectively.

The correspondence between E_{Si} and $E_{\text{c.m.}}$ can be fitted using the least-squares method with a linear function, as expressed in Eq. (2). As shown in Fig. 5, the red and black dots approximately follow straight lines.

$$E_{\text{c.m.}}(x) = E_{\text{Si}}(x) \cdot k + b, \tag{2}$$

Step 3: Subtract the background events from the energy spectrum in the frame of the center of mass. Corrections for the beam particle and ^{12}C atom numbers are required for the carbon-induced background. The (CH$_2$)$_n$ and carbon targets have different energy stopping powers for ^{23}Na. The correction factor f_n for the ^{12}C atom numbers is the ratio of the number of C atoms corresponding to 1 keV of energy deposited in the (CH$_2$)$_n$ target and the carbon target for the same energy of the ^{23}Na beam. This relationship was calculated using LISE++ and fitted to a linear function (Fig. 6.

$$dm_c/dE_{\text{c.m.}} = E_{\text{c.m.}} \cdot k_c + b_c, \tag{3}$$

$$dm_{(\text{CH}_2)_n}/dE_{\text{c.m.}} = E_{\text{c.m.}} \cdot k_{(\text{CH}_2)_n} + b_{(\text{CH}_2)_n}, \tag{4}$$
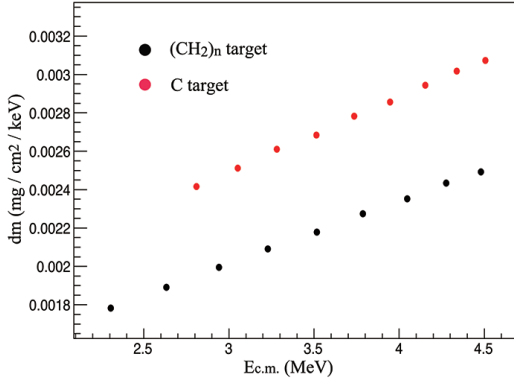
Fig. 6. (Color online) Relationship between the bin target thickness and center-of-mass energy.

$$f_{\mathrm{n}} = \frac{E_{\mathrm{c.m.}} \cdot k_{(\mathrm{CH_2})_{\mathrm{n}}} + b_{(\mathrm{CH_2})_{\mathrm{n}}}}{E_{\mathrm{c.m.}} \cdot k_{\mathrm{c}} + b_{\mathrm{c}}} \qquad (5)$$

The number of ^{12}C atoms corresponding to each bin of the carbon target and the $(\mathrm{CH_2})_{\mathrm{n}}$ target energy spectra is given by Eq. (3) and Eq. (4). The correction factor f_{n} is given by Eq. (5). Subsequently, the carbon background can be subtracted from the energy spectrum of p_0. As shown in Fig. 7, the black line represents the energy spectrum of the $(\mathrm{CH_2})_{\mathrm{n}}$ target and the red line represents the energy spectrum of the carbon target. The net energy spectrum of the $^1\mathrm{H}(^{23}\mathrm{Na}, p)^{23}\mathrm{Na}$ channel can be obtained by subtracting the normalized carbon background.
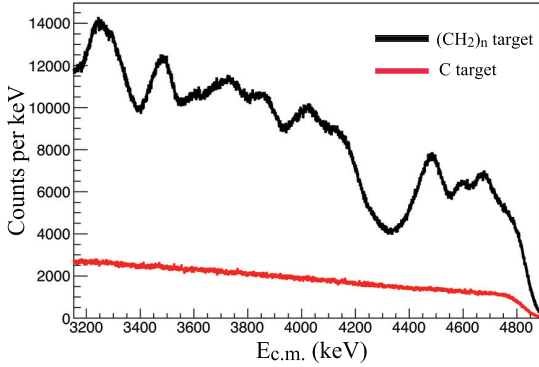

Fig. 7. (Color online) Yields from $^1\mathrm{H}(^{23}\mathrm{Na}, p_0)^{23}\mathrm{Na}$ elastic scattering channel. The background from the pure carbon target is flat without any resonance structure.

Step 4: Calculate the excitation function of $^1\mathrm{H}(^{23}\mathrm{Na}, p)^{23}\mathrm{Na}$, based on the net yield of p_0 exit channel. Because each bin in the p_0 energy spectrum corresponds to different H atom numbers of the $(\mathrm{CH_2})_{\mathrm{n}}$ target, the differential cross-section needs to be calculated separately for each energy point. The excitation functions of the proton and α channels are shown in Fig. 8 and Fig. 9, respectively, according to Eq. (6).

$$d\sigma/d\Omega = \frac{N_{\mathrm{count}}}{N_{\mathrm{H}} \cdot N_{\mathrm{I}} \cdot \Omega} \qquad (6)$$

where N_{H} and N_{I} represent the numbers of H atoms in the target and incident $^{23}\mathrm{Na}^{9+}$ beam ions, respectively. Ω denotes the solid angle of the Si detector.
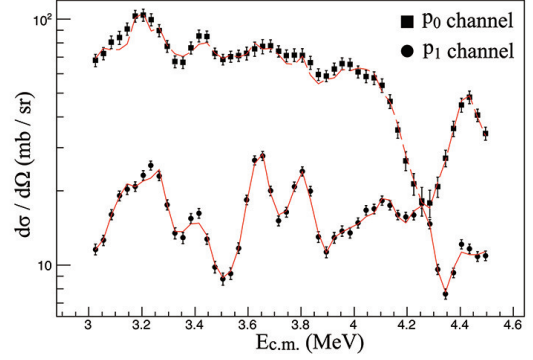

Fig. 8. (Color online) Excitation function for the proton exit channels. p_0 and p_1 represent $^1\mathrm{H}(^{23}\mathrm{Na}, p_0)^{23}\mathrm{Na}$ and $^1\mathrm{H}(^{23}\mathrm{Na}, p_1)^{23}\mathrm{Na}^*_{440}$, respectively.
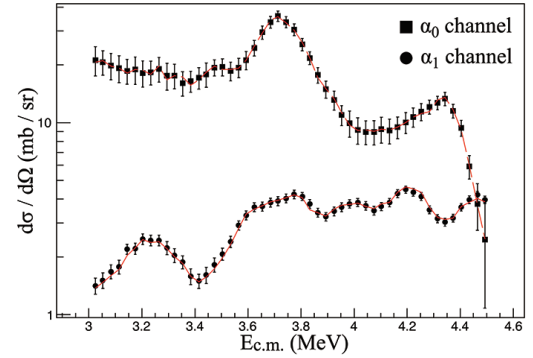
Fig. 9. (Color online) Excitation function for the α exit channels. α_0 and α_1 represent $^1\mathrm{H}(^{23}\mathrm{Na}, \alpha_0)^{20}\mathrm{Ne}$ and $^1\mathrm{H}(^{23}\mathrm{Na}, \alpha_1)^{20}\mathrm{Ne}^*_{1634}$, respectively.

Throughout the data analysis process, each step resulted in an error that was ultimately contained in the individual data points of the excitation function. These errors mainly include γ-charged-particle coincidence, statistical, carbon background deduction, and p_1 (α_1) deduction errors in the p_0 (α_0) calculations. For γ-particle coincidence, the coincidence efficiency mainly depends on the γ detection efficiency, silicon efficiency, and accidental coincidence events. The errors of these factors were independent. The γ detection efficiency error evaluated through the Geant4 simulation process was less than 3%, whereas the silicon detection efficiency error was negligible. Accidental coincidence events were uniformly distributed in the coincidence time spectrum and were

evaluated as having an error of less than 2%. Before the carbon background deduction, the energy spectrum must be divided into individual bins, with statistical errors assigned to each bin. For energy points with low counts, the statistical error was relatively large, close to 2%. The error after carbon background deduction depends on statistical errors and errors introduced during the subtraction process. During carbon background deduction, the ratio of carbon background counts to total counts positively correlated with the error introduced by the subtraction process. As shown in Fig. 7, for the p_0 channel, the error after carbon background subtraction at 3.8 MeV was 5%. By comparison, for most energy points with lower background contributions, the error after background subtraction was approximately 3.5%. For the $p_0(\alpha_0)$ channel, similar errors caused by data processing were introduced when subtracting the $p_1(\alpha_1)$ channel. The γ-efficiency error must be considered separately when calculating the final error in the $p_1(\alpha_1)$ channel. Overall, the two subtraction processes were the main sources of excitation function errors. The total errors for p_1 and α_1 were less than 8% and 10%, respectively. p_0 and α_0 errors were correspondingly larger, that is, less than 10% and 17% over the entire energy range.

The R-matrix theory [50, 51] is a parametric framework that describes compound nuclear reactions and theoretically describes the resonance phenomena in nuclear reactions. For excitation functions that include resonance states, R-matrix analysis can decompose the differential cross section into three overlapping components: hard-sphere scattering background, independent resonances, and interference of multiple resonances. This study provided the exit-channel excitation functions of the compound nucleus ^{24}Mg populated by the ^{23}Na+p entrance channel. The Azure package was used to extract a series of exit channel resonance parameters related to the ^{12}C+^{12}C fusion reaction. The fitting results are indicated by the red lines in Fig. 8 and Fig. 9. The fitting results indicate that nearly 50 ^{24}Mg resonances are included

to reproduce the excitation functions, not only the 0^+ and 2^+ resonance levels relevant to the ^{12}C+^{12}C fusion reaction, but also other levels such as 1^- and 3^-. The ^{24}Mg resonances observed in the ^{23}Na+p entrance channel are very complex and discrete, but densely packed in the energy region of ^{12}C+^{12}C Gamow window. However, the resonance parameters of the proton and α decay channels are useful for the further study of the ^{12}C+^{12}C fusion reaction. The detailed results of the R-matrix analysis and its impact on the ^{12}C+^{12}C astrophysical S factor will be presented in a forthcoming paper [52].

V. SUMMARY

The thick-target inverse kinematics method is widely used to measure the excitation functions of $p(\alpha)$ elastic and inelastic scattering induced by radioactive ion beams. In this study, the conventional TTIK method was extended to include complex reaction channels for the first time, which enables the simultaneous extraction of the excitation functions of different reaction channels. The high energy resolution and high detection efficiency γ - charged particle coincidence are essential for promoting this novel method for radioactive ion beam-induced reactions. Although the ^{24}Mg resonances observed in this study were useful, they were largely beyond the relevance of the ^{12}C+^{12}C fusion reaction. A similar measurement utilizing ^{20}Ne+α can be performed to significantly reduce ^{24}Mg resonances in the excitation functions.

[1] S.E. Woosley, A. Heger, and T.A. Weaver, The evolution and explosion of massive stars. Rev. Mod. Phys. **74**, 1015 (2002). doi: 10.1103/RevModPhys.74.1015

[2] A. Cumming and L. Bildsten, Carbon flashes in the heavy-element ocean on accreting neutron stars. Astrophys. J. **559**, L127–L130 (2001). doi: 10.1086/323937

[3] X.D. Tang and L.H. Ru, The ^{12}C+^{12}C fusion reaction at stellar energies. EPJ Web Conf. **260**, 10 (2022). doi: 10.1051/epjconf/202226001002

[4] K. Mori, M.A. Famiano, T. Kajino, Impacts of the new carbon fusion cross-sections on type Ia supernovae. MNRAS: Letters **482**, L70–L74 (2019). doi: 10.1093/mnrasl/sly188

[5] Z.H. Li, G.X. Li, H.K. Wang et al., Supernovae and their scientific secrets. Nucl. Tech. (in Chinese) **46**, 195–200 (2023). doi: 10.11889/j.0253-3219.2023.hjs.46.080021

[6] B.B. Back, H. Esbensen and C.L. Jiang et al., Recent developments in heavy ion fusion reactions. Rev. Mod. Phys. **86**, 317–360 (2014). doi: 10.1103/RevModPhys.86.317

[7] T.E. Strohmayer and E.F. Brown, A remarkable 3 hour thermonuclear burst from 4u 1820-30. Astrophys. J. **566**, 1045–

1059 (2002). doi: 10.1086/338337

[8] J.R. Patterson, H. Winkler, C.S. Zaidins et al., Experimental investigation of the stellar nuclear reaction ^{12}C $+^{12}$ C at low energies. Astrophys. J. **157**, 367 (1969). doi: 10.1086/150073

[9] H.W. Becker, K.U. Kettner, C. Rolfs et al., The ^{12}C $+^{12}$ C reaction at sub-coulomb energies (II). Z. Phys. A **303**, 305–312 (1981). doi: 10.1007/BF01421528

[10] J. Zickefoose, A.D. Leva, F. Strieder et al., Measurement of the ^{12}C(^{12}C$, p$)^{23}Na cross section near the Gamow energy. Phys. Rev. C **97**, 065806 (2018). doi: 10.1103/PhysRevC.97.065806

[11] E.F. Aguilera, P. Rosales, E. Martinez-Quiroz et al., New γ-ray measurements for ^{12}C $+^{12}$ C sub-coulomb fusion: Toward data unification. Phys. Rev. C **73**, 064601 (2006). doi: 10.1103/PhysRevC.73.064601

[12] T. Spillane, F. Raiola, C. Rolfs et al., ^{12}C+^{12}C fusion reactions near the Gamow energy. Phys. Rev. Lett. **98**, 122501 (2007). doi: 10.1103/PhysRevLett.98.122501

[13] L. Barrón-Palos, E.F. Aguilera, and J. Aspiazu et al., Absolute cross sections measurement for the ^{12}C $+^{12}$ C system at astrophysically relevant energies. Nucl. Phys. A **779**, 318 (2006).

doi: 10.1016/j.nuclphysa.2006.09.004

[14] Z.L. Shen, J.J. He, Study of primordial deuterium abundance in Big Bang nucleosynthesis. Nucl. Sci. Tech. **35**, 63 (2024). doi: 10.1007/s41365-024-01423-3

[15] M.D. High and B. Cujec, The $^{12}C +^{12}C$ sub-coulomb fusion cross section. Nucl. Phys. A **282**, 181–188 (1977). doi: 10.1016/0375-9474(77)90179-8

[16] B. Bucher, X.D.Tang and X. Fang et al., First direct measurement of $^{12}C(^{12}C, n)^{23}Mg$ at stellar energies. Phys. Rev. Lett. **114**, 251102 (2015). doi: 10.1103/PhysRevLett.114.251102

[17] A. Tumino, C. Spitaleri, M. L. Cognata et al., An increase in the $^{12}C +^{12}C$ fusion rate from resonances at astrophysical energies. Nature **557**, 687–690 (2018). doi: 10.1038/s41586-018-0149-4

[18] G.R. Caughlan and W.A. Fowler, Thermonuclear Reaction Rates V.. Atom. Data Nucl. Data. **40**, 1 (1988). doi: 10.1016/0092-640X(88)90009-5

[19] N.T. Zhang, X.Y. Wang and D. Tudor et al., Constraining the $^{12}C+^{12}C$ astrophysical S-factors with the $^{12}C+^{13}C$ measurements at very low energies. Phys. Lett. B **801**, 135170 (2020). doi: 10.1016/j.physletb.2019.135170

[20] A. Diaz-Torres and M. Wiescher, Characterizing the astrophysical s factor for $^{12}C +^{12}C$ fusion with wave-packet dynamics. Phys. Rev. C **97**, 055802 (2018). doi: 10.1103/PhysRevC.97.055802

[21] M. Assuncao and P. Descouvemont, Role of the hoyle state in $^{12}C +^{12}C$ fusion. Phys. Lett. B **723**, 355–359 (2013). doi: 10.1016/j.physletb.2013.05.030

[22] H. Esbensen, X. Tang and C.L. Jiang, Effects of mutual excitations in the fusion of carbon isotopes. Phys. Rev. C **84**, 064613 (2011). doi: 10.1103/PhysRevC.84.064613

[23] C.L. Jiang, D. Santiago-Gonzalez, S. Almaraz-Calderon et al., Reaction rate for carbon burning in massive stars. Phys. Rev. C **97**, 012801 (2018). doi: 10.1103/PhysRevC.97.012801

[24] C.L. Jiang, K.E. Rehm and R.V.F. Janssens et al., Influence of Nuclear Structure on Sub-Barrier Hindrance in Ni+Ni Fusion. Phys. Rev. Lett. **93**, 012701 (2004). doi: 10.1103/PhysRevLett.93.012701

[25] C.L. Jiang, B.B. Back, K.E. Rehm et al., Heavy-ion fusion reactions at extreme sub-barrier energies. Eur. Phys. J. A **57**, 235 (2021). doi: 10.1140/epja/s10050-021-00536-2

[26] A. Galindo-Uribarri, J. Gomez del Campo, J.R. Beene et al., Study of resonant reactions with radioactive ion beams. Nucl. Instr. and Meth. B **172**, 647–654 (2000). doi: 10.1016/S0168-583X(00)00220-2

[27] Shigeru Kubono, Experimental determination of astrophysical reaction rates with radioactive nuclear beams. Nucl. Phys. A **693**, 221–248 (2001). doi: 10.1016/S0375-9474(01)01140-X

[28] J.J. He, S. Kubono, T. Teranishi et al., Investigation of structure in ^{23}Al via resonant proton scattering of $^{22}Mg + p$ and the $^{22}Mg(p, \gamma)^{23}Al$ astrophysical reaction rate. Phys. Rev. C **76**, 055802 (2007). doi: 10.1103/PhysRevC.76.055802

[29] J.J. He, P.J. Woods, T. Davinson et al., Measurement of the inelastic branch of the $^{14}O(\alpha, p)^{17}F$ reaction: Implications for explosive burning in novae and x-ray bursters. Phys. Rev. C **80**, 042801(R) (2009). doi: 10.1103/PhysRevC.80.042801

[30] J.J. He, S. Kubono, T. Teranishi et al., Investigation of excited states in ^{22}Mg via resonant elastic scattering of $^{21}Na+p$ and its astrophysical implicationss. Phys. Rev. C **80**, 015801 (2009). doi: 10.1103/PhysRevC.80.015801

[31] J.J. He, L.Y. Zhang, A. Parikh et al., The $^{18}Ne(\alpha, p)^{21}Na$ breakout reaction in x-ray bursts: Experimental determination of spin-parities for α resonances in ^{22}Mg via resonant elastic

scattering of $^{21}Na + p$. Phys. Rev. C **88**, 012801(R) (2013). doi: 10.1103/PhysRevC.88.012801

[32] Y.B. Wang, B.X. Wang, X. Qin et al., $^{13}N+p$ elastic resonance scattering via a thick-target method. Phys. Rev. C **77**, 044304 (2008). doi: 10.1103/PhysRevC.77.044304

[33] T. Teranishi, S. Kubono, S. Shimoura et al., Study of resonance states in ^{12}N using a radioactive ion beam of ^{11}C. Phys. Lett. B **556**, 27–32 (2003). doi: 10.1016/S0370-2693(03)00098-4

[34] C. Ruiz, T. Davinson, F. Sarazin et al., Multichannel R-matrix analysis of elastic and inelastic resonances in the $^{21}Na + p$ compound system. Phys. Rev. C **71**, 025802 (2005). doi: 10.1103/PhysRevC.71.025802

[35] G.V. Rogachev, P. Boutachkov, A. Aprahamian et al., Analog States of ^7He Observed via the $^6He(p, n)$ Reaction. Phys. Rev. Lett. **92**, 232502 (2004). doi: 10.1103/PhysRevLett.92.232502

[36] Y.B. Wang, B.X. Wang, X.X. Bai et al., A Setup for Resonance Scattering Reactions with Thick Target. HEP & NP **30**(Suppl. II), 202 (2006). doi: fileZGWLC/journal/article/zgwlc/2006/S2/PDF/HJG2006-57.pdf

[37] X. Qin, Y.B. Wang, X.X. Bai et al., Levels in ^{13}N examined by $^{12}C + p$ elastic resonance scattering with thick target. Chin. Phys. C **32**, 957 (2008). doi: 10.1088/1674-1137/32/12/004

[38] Y.B. Wang, X. Qin, B.X. Wang et al., Simulation and analysis of $^{13}N + p$ elastic resonance scattering. Chin. Phys. C **33**, 181 (2009). doi: 10.1088/1674-1137/33/3/004

[39] S.J. Jin, Y.B. Wang, B.X. Wang et al., Excited states in ^{18}Ne studied via $^{17}F + p$. Chin. Phys. Lett. **27**, 032102 (2010). doi: 10.1088/0256-307X/27/3/032102

[40] X. Liu, Y.B. Wang, Z.H. Li et al., Angular distribution of $^6He + p$ elastic scattering. Chin. Phys. C **36**, 716 (2012). doi: 10.1088/1674-1137/36/8/006

[41] S.J. Jin, Y.B. Wang, J. Su et al., Resonant scattering of $^{22}Na + p$ studied by the thick-target inverse-kinematic method. Phys. Rev. C **88**, 035801 (2013). doi: 10.1103/PhysRevC.88.035801

[42] Y.J. Chen, L.Y. Zhang, Examining the fluorine overabundance problem by conducting Jinping deep underground experiment. Nucl. Tech. (in Chinese) **46**, 110501 (2023). doi: 10.11889/j.0253-3219.2023.hjs.46.110501

[43] J.X. Yu, The IAE Peking HI-13 tandem accelerator. Nucl. Instr. and Meth. **184**, 157–159 (1981). doi: 10.1016/0029-554X(81)90862-4

[44] Y.M. Tian, J.X. Yu and Z.Y. liu et al., Progress report on the HI-13 tandem accelerator. Nucl. Instr. and Meth. A **244**, 39–47 (1986). doi: 10.1016/0168-9002(86)90734-5

[45] J.Y.H. Li, Y.J. Li, Z.H. Li et al., Nuclear astrophysics research based on HI-13 tandem accelerator. Nucl. Tech. (in Chinese) **46**, 30–42 (2023). doi: 10.11889/j.0253-3219.2023.hjs.46.080002

[46] W.P. Liu, Review of the development of tandem accelerator laboratory in 35 years. Nucl. Tech. (in Chinese) **46**, 201–206 (2023). doi: 10.11889/j.0253-3219.2023.hjs.46.080022

[47] K.N. Li, C.X. Kan, X.F. Wang et al., Practice and innovation in the operation and maintenance of HI-13 tandem accelerator for 35 years. Nucl. Tech. (in Chinese) **46**, 63–69 (2023). doi: 10.11889/j.0253-3219.2023.hjs.46.080005

[48] S. Agostinelli, J. Allison and K. Amako et al., Geant4–a simulation toolkit. Nucl. Instr. and Meth. B **506**, 250–303 (2003). doi: 10.1016/S0168-9002(03)01368-8

[49] Z. Kis, B. Fazekas and J. Östör et al., Comparison of efficiency functions for Ge gamma-ray detectors in a wide energy range. Nucl. Instr. and Meth. A **418**, 374–386 (1998). doi: 10.1016/S0168-9002(98)00778-5

[50] A.M. Lane and R.G. Thomas, R-matrix theory of nu-clear reactions. Rev. Mod. Phys. **30**, 257–353 (1958). doi:10.1103/RevModPhys.30.257

[51] P. Descouvemont and D. Baye, R-matrix theory of nu-clear reactions. Rep. Prog. Phys. **73**, 036301 (2010). doi:10.1088/0034-4885/73/3/036301

[52] W.K. Nan, Y.B. Wang, J. Su et al., Determination of resonances in Gamow window for $^{12}C+^{12}C$ fusion reaction via thick target inverse kinematics method. Phys. Lett. B, submitted.